



# Hydrothermal carbonization of corncob for hydrochar production and its combustion reactivity in a blast furnace

Qi An<sup>1</sup> · Qi Wang<sup>2</sup> · Jinpeng Zhai<sup>1</sup>

Received: 1 December 2023 / Accepted: 25 January 2024 / Published online: 6 February 2024  
© The Author(s), under exclusive licence to Springer-Verlag GmbH Germany, part of Springer Nature 2024

## Abstract

A key factor restricting the application of biochar in the steel industry is its high-quality upgrading. This paper evaluated the characteristics of hydrochar produced by HTC (hydrothermal carbonization) process of corncob to be used as a solid fuel. HTC temperatures (240–300 °C) and HTC water-reused times (1–3 times) were examined for their effects on hydrochar yield, physicochemical characteristics, and combustion properties. The results showed hydrochar yields, O/C, and H/C parameters decreased as HTC temperature and water-reused times increased, while its high heating value increased. Due to dehydration and decarboxylation, hydrochar showed similar characteristics to those in bituminous coal. The removal efficiency of alkali metal K reached 99% after HTC treatment. Carbonaceous hydrochar had become more compact, orderly, and stable with increasing amounts of aromatic functional groups, C=C, and C=O. Hydrochar, as a biofuel, has higher ignition energy and is more stable than corncob due to its high carbonaceous order degree. To calculate combustion kinetic parameters, the Kissinger–Akahira–Sunose (KAS) and Flynn–Wall–Ozawa (FWO) methods were applied. The results revealed that  $E_{\alpha}$  (average activation energy) was quite similar between the two models. HC-300 had an  $E_{\alpha}$  of 262 kJ/mol. HTC could be an efficient way to reutilize corncob biomass into clean biofuels with high calorific value.

**Keywords** Hydrothermal carbonization · Corncob · Hydrochar · Combustion characteristics · Combustion kinetic parameters

## Introduction

With the increasingly serious problem of global warming caused by the use of fossil energy, the low-carbon utilization of energy has become a research hotspot. In order to solve energy and environmental problems, it is of vital importance to find a new energy source to meet the energy demand (Crutzen et al. 2008; McGlade and Ekins 2015).

Corn cob is one of the main crop wastes (Trninic et al. 2016). The thermochemical conversion method is more economical, environmentally friendly, and efficient among the

existing biomass treatment technologies (Chen et al. 2015). However, alkali metals, ash, etc. can easily cause pollution (Li et al. 2012). It is crucial to give impetus to the development of effective removal of ash and harmful alkali metal elements (K, Na, etc.) technology for better sustainable high-value utilization of corncob.

Hydrothermal carbonization (HTC) is an extremely effective biomass treatment method and has a long history of development. The efficient utilization of HTC treatment not only increases the value of biomass but also reduces the emission of carbon dioxide and pollutants, which is conducive to the realization of green energy utilization (Funke et al. 2013; Abdul Quader et al. 2016; Zhu et al. 2016). Compared with the traditional direct incineration and pyrolysis of biomass, HTC treatment takes advantage of the critical state property of water, which makes raw biomass materials undergo a series of reactions at relatively low temperature (180–300 °C) and relatively high pressure (2–30 MPa) under the condition of isolated air, including dehydration, condensation, aromatization, and other hydrolysis processes,

Responsible Editor: Zhihong Xu

✉ Jinpeng Zhai  
zhaijinpeng@sjtu.edu.cn

<sup>1</sup> Institute of Thermal Energy Engineering, School of Mechanical Engineering, Shanghai Jiao Tong University, Shanghai 200240, China

<sup>2</sup> School of Energy and Power Engineering, Jiangsu University, Zhenjiang 212013, Jiangsu, China

and finally form hydrochar (Mumme et al. 2011; Gao et al. 2015).

Mkel et al. (Mäkelä et al. 2018) reported that the HTC technology treatment method can take advantage of the properties of subcritical water, which dissolves the sample resulting in an increase in the fixed carbon content of the hydrochar. Wu et al. found that hydrochar showed a 40% increase in C content because of carbon densification in HTC (Wu et al. 2023). Meanwhile, hydrochar has abundant functional groups and carbon content, which makes it useful as a potential nanomaterial (Titirici and Antonietti 2009). By improving porosity through HTC (Falco et al. 2013), and immobilizing heavy metals (Wagner and Kaupenjohann 2014), it could also be used as an electrode material for electrochemical supercapacitors (Ding et al. 2013; Patrinoiu et al. 2015; Liu et al. 2022) or activated carbon materials (Lin et al. 2021).

HTC treatment is beneficial for effective removal of ash and harmful alkali metal elements. Tekin et al. (Tekin et al. 2014) found that HTC treatment not only increased the carbon content in the produced solids but also reduced the ash content due to the presence of aqueous solutions. Li et al. (Li et al. 2020) reviewed the nitrogen removal effect of HTC process and suggested that 60% of N in the raw material was transferred to the liquid phase product, which resulted in a significant reduction in NO<sub>x</sub> emissions during hydrochar combustion.

Besides, HTC treatment could effectively improve the quality and sustainably re-utilize biomass converted into clean coal-like solid fuel (Wang et al. 2020b). Research by Lokahita et al. (Baskoro Lokahita et al. 2017) found that HTC was a new way to improve the calorific value of biochar. With HTC treatment, the HHV of the biomass hydrochar increased to 25.22 MJ/kg, which was comparable to lignite and bituminous coal. HTC treatment of different feedstocks was performed by Nzediegwu et al. (Nzediegwu et al. 2021). The experimental results showed that the hydrochar produced from lignocellulosic biomass at 240 and 300 °C was similar to highly volatile bituminous coal. Prawisudha et al. (Prawisudha et al. 2012) conducted many HTC experiments, and the results showed that the HTC process can effectively remove the amount of alkali metal and Cl (such as soluble potassium and sodium salts) in the raw material, and form a solid fuel with properties similar to sub-bituminous coal.

At the same time, because of the prominent combustion potential of hydrochar, some scholars had also conducted research on the combustion kinetics of hydrochar. Zhu et al. (Zhu et al. 2019) conducted a study on the combustion kinetics of cotton stalk biomass hydrochar, and the results showed that HTC treatment can effectively improve the HHV of the sample, and generate combustion materials with high compressive strength and high relaxation density. Peng et al.

(Peng et al. 2016) used the hydrothermal carbonization method to treat the sludge, and studied the characteristics and combustion behavior of the hydrothermal carbon. The results showed that HTC can reduce the O/C H/C atomic ratio, and the optimal solid fuel obtained by kinetics is 260 °C-60 min.

The operating conditions of HTC are important factors affecting hydrochar. Wang et al. (Wang et al. 2023) analyzed the effect of temperature and catalysts on HTC treatment and the results showed that adding catalysts Fe(NO<sub>3</sub>)<sub>3</sub>·9H<sub>2</sub>O and circulating water can improve the quality of hydrochar. Uddin et al. (Uddin et al. 2014) studied the effect of HTC reaction temperature (200 °C, 230 °C, 260 °C) and reaction circulating water process on Loblolly pine solid hydrochar products, the results showed that the HTC temperature and circulating water had a significant impact on the structure, chemical properties, and fuel properties of hydrochar, and the reason is that the acidic substances and suspended solids in the solution are released each time the solution is recycled. Mau et al. suggested that recirculation of the aqueous phase could improve the removal of alkali metal elements (Mau et al. 2019). However, few studies have been conducted on the characterizations and pellet combustion kinetics of Henan Corn cob (HC) hydrochar from HTC at different temperatures and reused water times. The main objective of this study is to develop HTC treatment methods to convert HC into clean solid products. There are three main purposes: (1) to evaluate the feasibility of HTC treatment for the conversion of HC into clean fuels, including searching for optimal HTC conditions; (2) to study the physicochemical properties, structure, and combustion characteristics of hydrochar; (3) to use kinetic simulations FWO and KAS methods to assess the ability of water carbon to be used as a fuel. The results could promote the application of biomass resources in the field of energy combustion. The physicochemical characteristics of hydrochar and kinetic simulations in this paper will promote the production of chemical and energy products by corn cob HTC.

## Experiment

### Materials

The HC was taken from a village in Henan Province, China. First, the HC samples were broken into small sizes of less than 2 cm by crushers. Then, HC was dried in a drying oven at 105 °C for 12 h. The proximate analysis was carried out according to GB/T212-2008 and GB-T476, and the elemental analysis was measured by a Vario EL cube analyzer. The proximate analysis of the HC showed the percentages of volatile (76.10%), ash (6.73%), and fixed carbon (17.17%). The ultimate analysis indicated that the percentages of C, H, N,

and S in the HC were 42.71%, 5.98%, 0.54%, and <0.01%, respectively. The percentage of O (44.05 wt.%) was obtained by difference.

## HTC experiment

HTC experiments of HC were performed in a 100 mL stainless steel hydrothermal reactor. A schematic diagram of the device is shown in Fig. 1. The HTC temperature and reaction time were controlled by PID controllers, respectively. The maximum test allowable pressure is 30 MPa, and the maximum allowable temperature is 400 °C. To analyze the effect of HTC temperature on HC. HTC experiments at 240 °C, 270 °C, 300 °C were performed on HC (HC-240, HC-270, and HC-300). In the next cycle of HTC experiments, the liquid collected from the initial experiment was used. In accordance with the procedure described above, sufficient supplemental water is added to make the total liquid mass five times the dry biomass. Repeat the same procedure for subsequent loop experiments. At each temperature, the quality of the collected liquid was almost constant with the number of cycles. The cosmetic water added in the cycle experiment was 40%, 36% and 29% of the total water required respectively.

In different HTC temperature experiments, HC feedstock 20 mg mixed with deionized water 60 ml. Reused water process is the initial experimental collection of circulating water 40 ml, adding deionized water 20 ml to replenish water, which is to achieve the material and liquid total mass ratio of 1:3. Repeat the same procedure for subsequent loop experiments. The total experiment time is 1 h. In order to explore the influence of the number of times of water reused, 1 time, 2 times, and 3 times were tested (HC-300–1, HC-300–2, and HC-300–3).

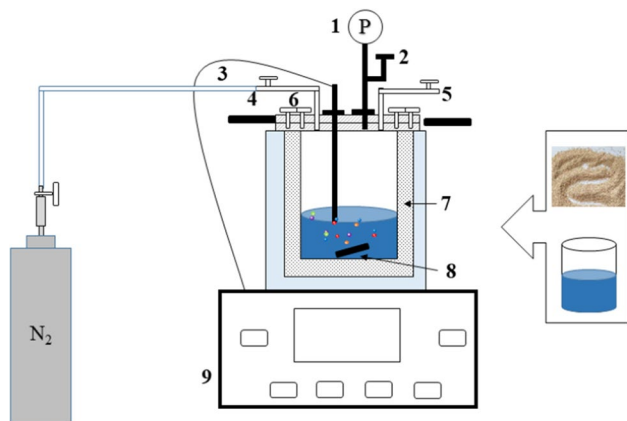


**Fig. 1** Lab-scale autoclave reactor schematic diagram: 1. Pressure gauge, 2. Explosion proof device, 3. Autoclave reactor, 4. Heating jacket, 5. Temperature sensor, 6. Magnetic stirrer, 7. PID controller, 8. Reactant, 9. Operation panel

## Physical and chemical characteristics analysis of hydrochars

Analytical techniques to determine the physicochemical properties of hydrochars have been described by Wang et al. (Wang et al. 2020b), this paper only makes a brief introduction. The microstructures of different hydrochars were observed using scanning electron microscopy (SEM). The chemical functional groups of different samples were determined by Fourier transform infrared (FTIR) analysis. The intrinsic carbonaceous structure of hydrochar was detected by Raman spectroscopy. Detection of Alkali Metal Elements in Samples by Inductively Coupled Plasma Optical Emission Spectrometer. Calculate the higher heating value (HHV), mass yield, and energy yield using the following equations (Channiwalla and Parikh 2002; Lin et al. 2015; Zhu et al. 2019):

$$\text{HHV} = 0.3137 \text{ C} + 0.7009 \text{ H} + 0.0318 \text{ O} - 1.3675 \quad (1)$$

Among them, C, H, N, O, and S represent the contents of carbon, hydrogen, nitrogen, oxygen, and sulfur, respectively.

$$\text{Mass yield} = \text{Mass of hydrochar} / \text{Mass of feedstock} \quad (2)$$

$$\text{Energy yield} = \text{Mass yield} \times \text{Energy densification} \quad (3)$$

$$\text{Energy densification} = \text{HHV of the hydrochar} / \text{HHV of the feedstock} \quad (4)$$

## Thermogravimetric analysis

Thermogravimetric analysis can be used to analyze the change law of sample weight with time and temperature. The thermogravimetric experiment of biomass was carried out with a German STA 449 F3 comprehensive thermal analyzer. The temperature rising rates were 5 °C, 10 °C, and 20 °C/min respectively. The temperature rises, from room temperature to 900 °C, and the equipment automatically records temperature and mass change data.

Using a thermogravimetric analyzer to study the weight loss process of the sample reaction, and using the weight loss curve DTG analysis to calculate the conversion rate  $\alpha$  of the reaction, using the following definition formula (Liu et al. 2012):

$$\alpha = \frac{m_1 - m_t}{m_0 - m_\infty} \quad (5)$$

where  $m_1$  is pre-reaction sample mass;  $m_t$  is sample mass at time  $t$ ;  $m_\infty$  is residual sample mass.

Combustibility index C and comprehensive combustion characteristic index S can be used to characterize the combustion characteristics of the sample (Li et al. 2011), and the calculation formula is shown below.

$$C = \frac{R_{\max}}{T_i^2} \quad (6)$$

$$S = \frac{R_{\max} R_{\text{mean}}}{T_i^2 T_f} \quad (7)$$

where  $R_{\max}$  is maximum combustion rate,  $S^{-1}$ ;  $R_{\text{mean}}$  is average combustion rate,  $S^{-1}$ ;  $T_i$  is the ignition temperature;  $T_m$  is the peak temperature;  $T_f$  is the burnout temperature.

### Kinetic analysis

Kinetics refers to all chemical kinetics that takes place in the reaction of substances, it can quantitatively analyze the chemical reaction rate and reaction-related influencing factors, and use the reaction-related mechanism to explain the experimental kinetics. The thermal analysis technique of the immobilized reactants can effectively conduct non-isothermal kinetic studies on the linear temperature process. The corresponding non-isothermal thermal reaction rate equation (Várhegyi 2007) is described as follows:

$$\frac{d\alpha}{dt} = k(T, P) \cdot f(\alpha) \quad (8)$$

where  $f(\alpha)$  is Mechanism Function of Reaction Model;  $t$  is Reaction time(s);  $k(T, P)$  is Reaction constant, related to temperature and pressure.

The Arrhenius equation,  $k(T, P)$  can be expressed as:

$$k(T) = A \cdot \exp\left(-\frac{E}{RT}\right) \quad (9)$$

where  $A$  is a pre-exponential factor( $s^{-1}$ ),  $E$  is activation energy(kJ/mol);  $R$  is the universal gas constant, 8.314 J/(mol K).

The reaction rate  $\beta$  is defined as

$$\beta = \frac{dT}{dt} = \frac{dT}{d\alpha} \cdot \frac{d\alpha}{dt} \quad (10)$$

Combining the above formula:

$$\frac{d\alpha}{dt} = \frac{A}{\beta} \cdot \exp\left(-\frac{E}{RT}\right) \cdot f(\alpha) \quad (11)$$

Integrating Eq. (8):

$$\int_0^\infty \frac{d(\alpha)}{f(\alpha)} = \frac{A}{\beta} \int_0^T \exp\left(-\frac{E}{RT}\right) dT \quad (12)$$

Defining the parameter  $u = \frac{E}{RT}$ , Eq. (8) can be expressed as:

$$\int_0^\infty \frac{d(\alpha)}{f(\alpha)} = \frac{AE}{\beta R} \int_u^\infty u^{-2} \exp(-u) du = \frac{AE}{\beta R} P(u) \quad (13)$$

Defining  $g(\alpha) = \int_0^\infty \frac{d(\alpha)}{f(\alpha)}$ , then Eq. (10) refers to:

$$g(\alpha) = \frac{AE}{\beta R} P(u) \quad (14)$$

According to the pyrolysis curve of HC, the kinetic parameters such as activation energy can be obtained by the method of equal conversion well. The parameters of the conversion method do not change with the heating rate, but only with the temperature. Therefore, this paper uses the Flynn–Wall–Ozawa (FWO) model and the Kissinger–Akahira–Sunose (KAS) (Fong et al. 2019) model to calculate the kinetic parameters, the formulas are as follows:

$$\ln\left(\frac{\beta}{T^2}\right) = \ln\left[\frac{AE}{Rg(\alpha)}\right] - \frac{E}{RT} \quad (15)$$

$$\ln(\beta) = \ln\left[\frac{AE}{Rg(\alpha)}\right] - 5.331 - 1.052 \frac{E}{RT} \quad (16)$$

## Results and discussion

### Mass and energy yields of hydrochar

Figure 2 illustrates that the hydrochar mass and energy yield of the HTC of HC at different temperatures and reused water times treatment. As the hydrothermal temperature increased from 240 to 300 °C, the mass yield of hydrochar decreased significantly from 54 to 38% and then to 31%, eventually. The yield reached the maximum in the range of 240–270 °C, which indicates that 240–270 °C is the violent reaction temperature range of HC hydrochar. A large amount of volatiles volatilize at this stage, so the yield of hydrochar drops

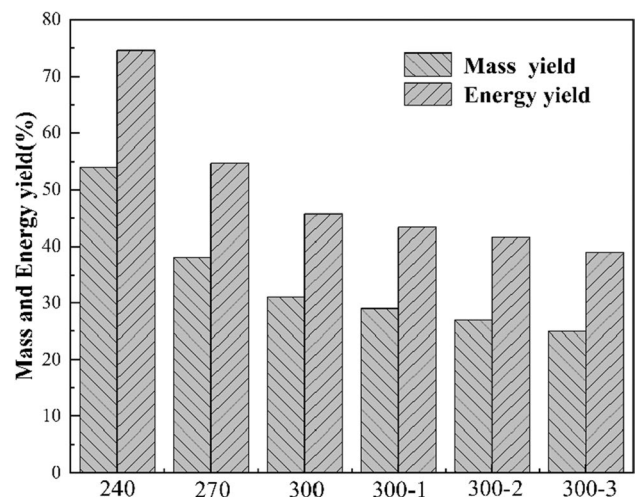


Fig. 2 Effects of HTC temperature and reused water times on the mass and energy yield

sharply. Besides, the experiment results showed that with the increase of water-reused times, the hydrochar mass yield decreased. However, the change in water reused times is not significant. In addition, acetic acid is produced in the solution after hydrothermal carbonization, which has a catalytic effect on the hydrothermal reaction process and reduces the yield of solid-phase products (Reza et al. 2015b; Zhou et al. 2021). Acetic acid can enhance hydrogen bond cleavage and degrade more cellulose. Therefore, the degradation reaction is accelerated to a certain extent, which is conducive to the occurrence of carbonization reaction, and hydrochar yield is reduced.

### Physical characteristics and HHV analysis of hydrochar

The atomic ratio and HHV of HC and hydrochars on the basis of the proximate and ultimate analysis, are shown in Table 1. HC had fixed carbon, volatile, and ash contents of 17.17%, 76.1%, and 6.73%, respectively. Hydrochar’s fixed carbon content increased as HTC temperatures and water reused times increased, however, its ash and volatile content decreased. HC-300–3 had an increase in the fixed carbon content to 61.25%, whereas the volatile of HC-300–3 dropped to 37.23% and ash content fell to 1.52%. The fundamental cause is that during the HTC process, HC undergoes dehydration and decarboxylation reactions. In general, these reactions result in main cause of composition changes. Meanwhile, when the HTC temperature rises, more volatile components are removed, resulting in more H<sub>2</sub>O and CO<sub>2</sub> being released. HTC operation continually dissolves water-soluble mineral components (such as K, Na, and Ca) into deionized water, which results in a decrease in the ash content in the hydrochar (Wang et al. 2020b). Adopting a suitable HTC temperature is a key factor in the production of hydrochar.

Based on the results of the ultimate analysis, it is evident that the C and O contents had changed dramatically from what they had been before. With C increasing from 42.71% in HC to 78.51% in HC-300–3 and O falling from 44.05 to

14.22%. HC-300–3 has a C content that is 83.8% higher than HC. The C and O content of HC-300–3 is comparable to that of bituminous coal injected into blast furnaces (da Silva Machado et al. 2010). Figure 2 revealed that variations in the content of C and O in hydrochar were gradual and mild when the HTC temperature exceeded 270 °C, suggesting that the chemical structure of hydrochar formed under these conditions would be more stable. The H content in the hydrochar was much lower than that in HC due to the dehydration and decarboxylation processes that happened during the HTC process, whereas the H content increased marginally with the increase of water-reused times. Dehydration and decarboxylation had little effect on N removal, as seen by the change in N content during HTC. Wang et al. (Wang et al. 2020b) noticed the same phenomenon when examining straw HTC treatment in their study. It was found that the number of water-reused times has little effect on the hydrochar produced under various operating conditions according to the approximate analysis and the ultimate analysis. This means that the number of HTC water reused times has little effect on the composition of hydrochar, which is mainly affected by HTC temperature. The selection of an appropriate HTC temperature is critical in the production of hydrochar.

Hydrochar is a product that has an increase in its HHV when the HTC temperature is increased and the number of water-reused times is increased in Table 1. The HHV in HC was only 17.84 MJ/kg, while reaching 26.02 MJ/kg in HC-300, and increasing to 27.49 MJ/kg in HC-300–3. The increasing HHV of hydrochar makes it more suitable as a blast furnace injection fuel (Chen et al. 2011). The HHV of hydrochar is related to the change of elements, as shown by Eq. (1). As a result of vigorous dehydration and decarboxylation during HTC treatment, several oxygen-containing functional groups were eliminated. As the minerals dissolve, the hydrochar’s ash content is reduced, thereby increasing its HHV. Both energy and mass yields have varied similarly in this process, as shown in Fig. 2. Hydrochar, due to its high HHV, has an energy yield that is in comparison to its mass yield of a higher level. The mass yield of HC-300–2 is only 27.8%, while its energy yield reaches 41.6%. For biomass

**Table 1** Proximate and ultimate analysis of hydrochar

Sample	Proximate analysis (wt.%)			Elemental analysis (wt.%)					H/C	O/C	HHV (MJ/kg)
	V <sub>d</sub>	A <sub>d</sub>	FC <sub>d</sub>	C	H	O <sub>d</sub>	N	S			
HC	76.10	6.73	17.17	42.71	5.97	44.05	0.54	<0.01	1.68	0.77	17.62
HC-240	59.18	1.47	39.35	67.99	5.07	25.11	0.36	<0.01	0.89	0.28	24.31
HC-270	49.59	1.94	48.47	71.88	5.03	20.18	0.34	<0.01	0.84	0.22	25.35
HC-300	42.61	1.67	55.72	73.94	5.04	18.93	0.42	<0.01	0.82	0.19	25.96
HC-300–1	41.83	1.58	56.59	75.03	5.1	17.87	0.42	<0.01	0.82	0.18	26.31
HC-300–2	38.84	1.53	59.63	77.65	5.22	15.18	0.42	<0.01	0.81	0.15	27.13
HC-300–3	37.23	1.52	61.25	78.51	5.34	14.22	0.41	<0.01	0.82	0.14	27.46



combustion technology, high energy yield can significantly reduce energy consumption in HTC processes and improve hydrochar utilization efficiency. The HC-300–2 hydrochar's volatile matter fell to 38.84% and the HHV increased to 27.13 MJ/kg when compared to HC. Hydrochar HC-300–2 showed similar HHV to those recorded in prior HTC studies for hyacinth, discarded eucalyptus bark, and wheat straw digestate (Gao et al. 2013, 2016; Reza et al. 2015a), although their heat values were moderately higher than sub-bituminous coal (25.53 MJ/kg)(Park and Jang 2011). Increasing HTC temperature further and water reused times further had little effect on lowering volatile matter content and raising hydrochar HHV. With the savings in energy and reduction in consumption, it makes sense to determine the HTC production condition at 300 °C and twice water reused times whose HHV has 27.13 MJ/kg.

Van Krevelen diagrams Fig. 3 show the atomic ratios of H/C and O/C of samples (Lee et al. 2018). In terms of the H/C and O/C, HC reaches a H/C of 1.68 and an O/C of 0.77, while HC-300–3 reaches 0.82 and 0.14, respectively. The properties of all HC hydrochars are similar to bituminous coal as a result of HTC treatment, and the higher the hydrothermal temperature and the more water-reused times, the more similar the features are. In the presence of dehydration and decarboxylation reactions, aromatics in hydrochar become continuously carbonized as the temperature increases. As a result, it leads to a decrease in the mass fraction of H and O while an increase in C. If HTC temperature is under 270 °C, however, H/C and O/C ratios are substantially influenced by the HTC temperature due to cellulose and hemicellulose in HTC are rapidly destroyed. Significant polycondensation and carbonization processes occur between highly stable components (such as lignin, etc.) if the temperature of HTC is more than 270 °C, resulting in

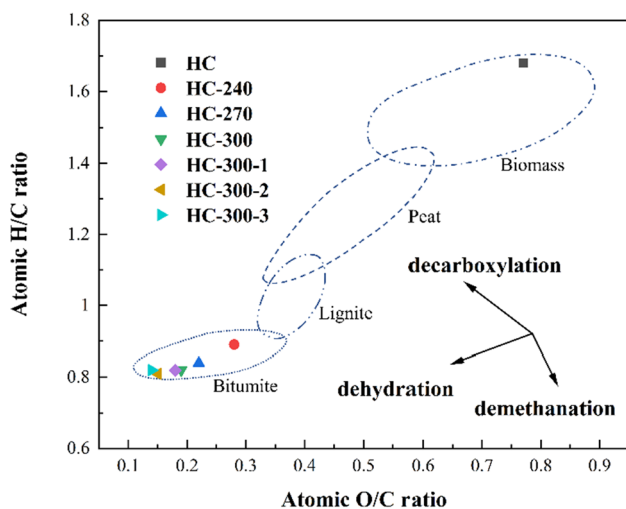


**Fig. 3** Van Krevelen diagram for HC and hydrochars

some minor changes in the mass proportions of C, H, and O of the hydrochar. The water-reused technology had little effect on O/C and H/C. When the influence of HTC water-reused times on O/C and H/C is compared, the O/C and H/C of the hydrochar made at 300 °C under different HTC water-reused times have little change and are basically in the range of 0.14–0.18 and 0.81–0.82. The O/C atomic ratios fell from 0.19 of HC-300 to 0.14 of HC-300–3. It was revealed that the HTC process involved decarboxylation, dehydration, and demethanation, with the dehydration reaction rate being higher than the decarboxylation reaction rate. As can be seen from Fig. 3, these ratios all fall in the bituminous coal region. The results demonstrate that the number of HTC water reused times has less effect on the hydrochar characteristics than HTC temperature.

The HC, HC-270 and HC-300–2 samples were tested by ICP element detection as shown in Table 2. It can be clearly seen that the HTC treatment is very effective in removing alkali metal elements from the samples. The removal efficiency of metal elements is all above 60%, especially the removal efficiency of K reaches 99%. The removal of metal elements can reduce the problem of combustion contamination in the combustion process.

### Chemical structure characteristics of hydrochar

FT-IR can analyze the types of functional groups in the sample. The changes of surface functional groups with reaction conditions can be explored by analyzing the samples (Seredych et al. 2008) FT-IR spectra with different HTC conditions are shown in Fig. 4.

The infrared spectra of the six samples are very similar. The absorption peaks of the HC sample include CH bending vibration peak ( $790\text{ cm}^{-1}$ ), CO common absorption peak ( $1060\text{ cm}^{-1}$ ), C–OH (phenol) ( $1200\text{--}1300\text{ cm}^{-1}$ ), C = C stretching vibration peak ( $1605\text{ cm}^{-1}$ ), C = O absorption peak ( $1735\text{ cm}^{-1}$ ),  $\text{CH}_n$  absorption peak ( $2840\text{--}3000\text{ cm}^{-1}$ ) and -OH absorption peak ( $3200\text{--}3500\text{ cm}^{-1}$ ) (Zhang et al. 2015). There are abundant functional groups in the original HC of corncob, and there are a large number of absorption peaks at  $1800\text{--}1000\text{ cm}^{-1}$ . It shows that there are abundant oxygen-containing functional groups in the original HC samples, such as hydroxyl, carboxyl, carbonyl, etc. Because

**Table 2** Dealkalization rate of samples

Sample	Dealkalization rate content of alkali elements (wt.%)				
	K	Mg	Al	Ca	Na
HC-270	99%	89%	87%	64%	88%
HC-300–2	99%	91%	88%	73%	94%

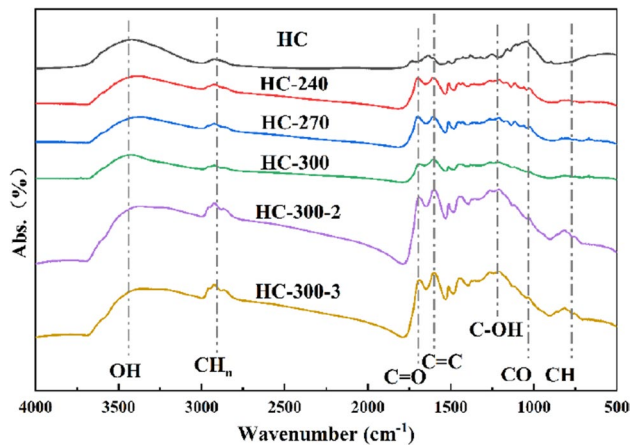


**Fig. 4** FTIR patterns of different samples

of the poor stability and high activity of these functional groups, HC is easily decomposed at low temperatures.

Due to the degradation of cellulose and hemicellulose, the CO absorption peak at  $1060\text{ cm}^{-1}$  gradually disappeared with the increase of HTC temperature and the number of water reused times, while the C=C stretching vibration and  $\text{CH}_n$  stretching vibration peaks gradually strengthened. The absorption peak at  $1605\text{ cm}^{-1}$  is the stretching vibration of the C=C bond on the aromatic ring. There is a strong absorption peak in the range of  $3600\text{--}3200\text{ cm}^{-1}$ , which is due to the vibrational stretching of functional groups -OH and - $\text{CH}_n$ , the asymmetric stretching of functional groups - $\text{CH}_3$  at  $2956\text{ cm}^{-1}$ , the asymmetric stretching of - $\text{CH}_2$  at  $2922\text{ cm}^{-1}$ , and the asymmetric stretching of fat. The absorption peaks generated by the stretching vibration of the group CO functional group in the range of  $1200\text{--}1000\text{ cm}^{-1}$  indicate the existence of oxygen-containing functional groups in cellulose. The weakening of the hydroxyl (-OH peak) is because of the removal of  $\text{H}_2\text{O}$  during the hydrothermal carbonizing process. When the hydrothermal temperature reached  $300\text{ }^\circ\text{C}$ , the peak corresponding to the carbonyl group (C=O) disappeared, because the carbonyl group was removed in the form of  $\text{CO}_2$ .

This fact suggests that the decarboxylation and the recombination in the HTC process resulted in the structure of hydrochar containing a large number of oxygen-rich organic functional groups and soluble oligomers. The structure of hydrochar by HTC has a highly aromatic, and it has functional groups such as C=C, C-H, and aliphatic substances. Some of the compounds dissolve and gradually aromatize because of the presence of subcritical water. These results are consistent with the decreasing of H/C and O/C atomic ratios as described above. The structure of aromatic ring is more stable and requires a higher temperature to be destroyed in combustion, which makes the combustion reactivity of hydrochar lower.

However, the ordering degree of the carbonaceous structure can't be only determined by the FT-IR analysis. Therefore, Raman analysis was tested for further analysis and the results are showed in Fig. 5. Raman can detect carbon structures within substances, and the internal characteristic structure of the material can be directly reflected through the spectral peaks (Rajaroo et al. 2014). The integrity of the  $\text{sp}^2$  hybrid bond structure in the graphite structure shows a G peak ( $1580\text{ cm}^{-1}$ ), while in amorphous carbonaceous materials it usually appears as a D peak ( $1360\text{ cm}^{-1}$ ) (Rajaroo et al. 2014), representing the defect sites of the graphitic structure (Mosqueda et al. 2019). The D peak was further resolved to four separate vibrational peaks,  $\text{D}_1$ ,  $\text{D}_2$ ,  $\text{D}_3$ , and  $\text{D}_4$ . In this study, the Lorentzian function method was used to analyze the  $\text{D}_1$ ,  $\text{D}_2$ ,  $\text{D}_4$ , and G peaks, while the Gaussian function was used to fit the  $\text{D}_3$  peak (Wang et al. 2020a).

One study (Rajaroo et al. 2014) showed that the  $I_{\text{D}_3+\text{D}_4}/I_{\text{G}}$  value could better characterize the ordering degree of carbonaceous structures. Comparing the  $I_{\text{D}_3+\text{D}_4}/I_{\text{G}}$  values of samples in Table 3, it can be found that with the increase in hydrothermal temperature and water-reused times, the value of  $I_{\text{D}_3+\text{D}_4}/I_{\text{G}}$  continues to decrease, and the carbonization ordering degree of HC hydrochar increases,  $\text{HC-240} > \text{HC-270} > \text{HC-300} > \text{HC-300-2}$ . Similar conclusions can be concluded from FT-IR analysis. Furthermore, the expansion of the aromatic ring structural units indicates that the sample is becoming more graphitized. The main reasons are that the side chains and oxygen-containing functional groups of substances such as polysaccharides in HC are more easily destroyed at high temperatures and the release of volatiles is more complete at high HTC temperatures. HTC treatment increased the carbonaceous crystallite size and graphitization degree of hydrochar, making the carbonaceous structure of hydrochar more compact, orderly, and stable.

### Combustion behavior of hydrochar

Thermogravimetric analysis was performed to investigate the combustion behavior of HC and hydrochars. Figure 6 depicts the reaction rate and combustion conversion of samples. PRE-HC is corncob that has not been treated with HTC.

There are three main stages with two peaks in the DTG curve of the PRE-HC, owing to differences in structure and thermal stability of lignin, cellulose, and hemicellulose (Wang et al. 2018). (1) The evaporating stage of water and low-boiling organic material; (2) the volatile combustion stage; and (3) the fixed carbon combustion stage (Khan et al. 2009). The low fixed carbon and high volatile content in the HC are contributed to the separation of sharp peaks during combustion, resulting in two peaks (Zhao et al. 2013; Wang et al. 2020b) The combustion transformation curves of hydrochars are shifted to the high-temperature

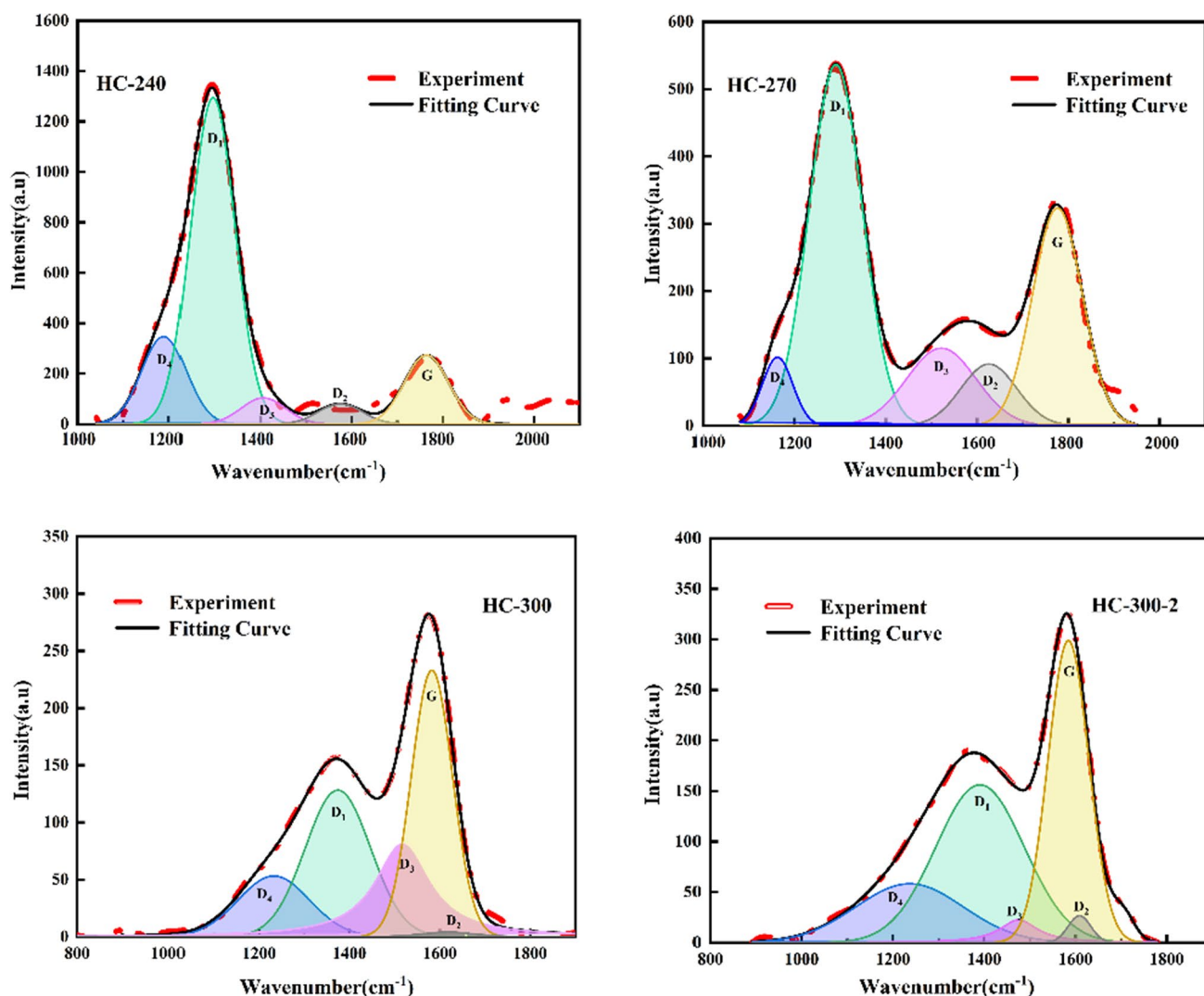


Fig. 5 Raman spectra of different samples

**Table 3** Microstructure parameters of different hydrochars

Sample	$I_{D1}$	$I_{D2}$	$I_{D3}$	$I_{D4}$	$I_G$	$I_{D3+D4}/I_G$
HC-240	103.9	1294.4	80.4	274.6	346.8	1.0899
HC-270	535.8	137.9	50.2	323.7	101.8	0.7405
HC-300	53.1	128.3	80.4	233.2	6.2	0.5751
HC-300-2	39.2	121.4	85.1	268.5	1.39	0.4558

range, with varied curve morphologies for different hydrochars. HC-240 and HC-270 have combustion transformation curves that are similar to PRE-HC, but two peaks are shifted to the high-temperature area. The basic reason for this is that the HTC process comprises decarboxylation and dehydration reactions, both of which lower the volatile content of hydrochar, resulting in a lower volatile combustion peak. When the HTC temperature reaches 300 °C, however, it's difficult to tell the difference between the

hydrochar and coal two combustions, because the DTG curve only has a single obvious peak of reaction rate, and the combustion temperature range and curve are similar to bituminous coal (Kizgut and Yilmaz 2004). When the temperature was 300 °C and the number of HTC water-reused times increases, the TG and DTG move to the high-temperature area. In particular, when HTC water is reused more than 2 times, the combustion curves overlap. These results suggest that raising HTC temperature has a greater



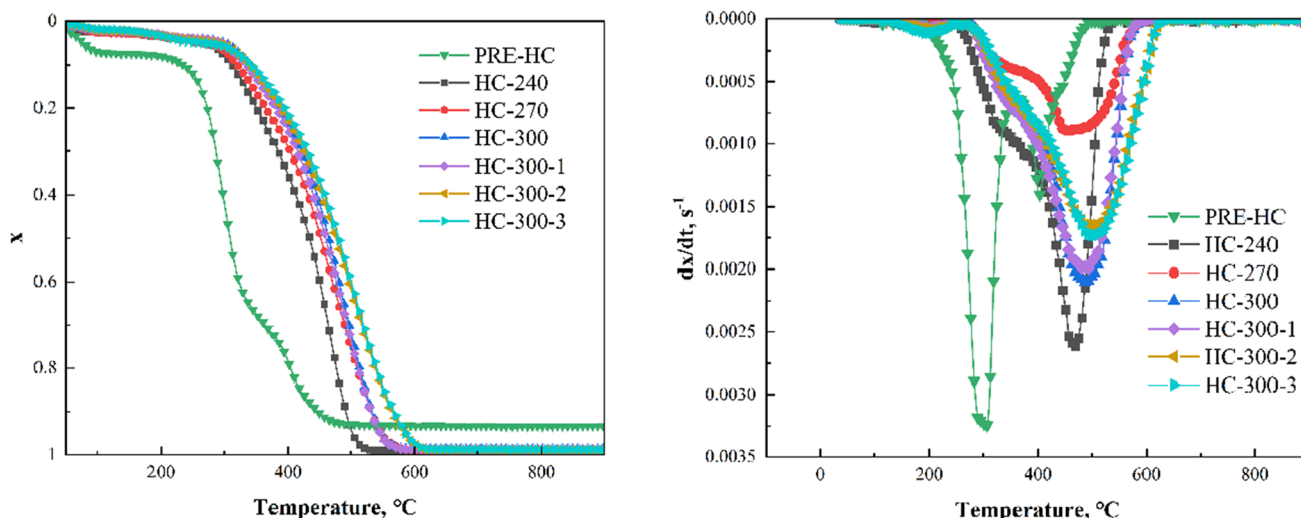


**Fig. 6** Experimental conversion and reaction rate curves of hydrochar with a heating rate( $\beta$ ) of 20 °C/min

impact on hydrochar combustion behavior than increasing HTC water reused times.

Several combustion characteristic parameters are defined to evaluate the combustion reactivity (Xu et al. 2010): initial temperature  $T_i$  (°C), peak combustion rate temperature  $T_m$  (°C), the maximum reaction rate  $(dx/dt)_{max}$  ( $s^{-1}$ ). Average reaction speed  $(dx/dt)_{mean}$  ( $s^{-1}$ ), burnout temperature  $T_f$  ( $s^{-1}$ ). Index C and S are calculated as shown in Sect. 2.4. Table 4 clearly shows the combustion characteristics parameters of different HC samples.

The PRE-HC demonstrated low  $T_i$  (248.1 °C) compared to all other hydrochars.  $T_i$  did not change significantly even when the HTC temperature was over 300 °C.  $T_i = 276.8$  °C for HC-240 and  $T_i = 299.2$  °C for HC-300, with a difference 22.4 °C.  $T_i = 299.2$  °C for HC-300 and  $T_i = 272.4$  °C for HC-300–3, with a difference 26.8 °C. Higher  $T_i$  can effectively avoid spontaneous combustion, and it is more conducive to storage and energy conversion (Peng et al. 2016; Wang et al. 2018). Comparing the  $T_m$  parameter, it was noticed that the  $T_m$  value corresponded to the devolatilization process and grew progressively as the HTC temperature and reused water times increased. The devolatilization

reaction peak vanished when the HTC conditions exceeded 270 °C due to decarboxylation and dehydration. The  $T_m$  value of the HC-240 sample was 434.8 °C and went up to 480.9 °C for HC-300–3. With the rise in HTC temperature and reused water times, the peak values of the combustion rate changed. Because of the dehydration and decarboxylation reaction in HTC, the value of  $(dx/dt)_{max}$  corresponding to  $T_m$  decreased as HTC temperature and reused water times increased. HTC treatment reduced the volatile carbon component of the hydrochar while increasing the fixed carbon content.

Comparing the  $T_f$  values in Table 4, it can be found that the  $T_f$  value increases with the increase of HTC temperature and water reused times, indicating that the hydrochars generated are more difficult to be burned out. This means that the combustion of these hydrochars requires longer times and higher temperatures with the increase of HTC temperature and water reused times. Overall, the combustion of hydrochar is expected to be more stable than combustion feedstocks with higher ignition points. Comparing the effects of HTC temperature and water reused times on the combustion characteristics of hydrochars, it can be found that HTC water

**Table 4** Combustion characteristics of different hydrochars samples

Sample	$\beta$ (°C/min)	$T_i$ (°C)	$T_m$ (°C)	$T_f$ (°C)	$(dx/dt)_{max}$ ( $s^{-1}$ )	$(dx/dt)_{mean}$ ( $s^{-1}$ )	$C \times 10^8$ ( $s^{-1} \cdot ^\circ C^{-2}$ )	$S \times 10^{14}$ ( $s^{-2} \cdot ^\circ C^{-3}$ )
PRE-HC	20	248.1	311.5	443.5	0.0033	8.77E-04	5.3254	10.5369
HC-240	20	276.8	434.8	504.6	0.0026	8.32E-04	3.4402	5.6719
HC-270	20	281.4	462.6	540.6	1.79E-03	8.72E-04	2.2602	3.6474
HC-300	20	299.2	464.8	550.4	0.0021	7.81E-04	2.3512	3.3381
HC-300–1	20	295.5	459.9	547.5	0.0020	6.12E-04	2.2807	2.5496
HC-300–2	20	287.9	476.3	584.7	0.0017	5.54E-04	2.0145	1.9099
HC-300–3	20	272.4	480.9	586.5	0.0017	5.03E-04	2.3415	2.0070

reused times have less effect on the combustion behavior of hydrochars. From the above TG combustion analysis, it can be seen that both increasing HTC temperature and water reused times will reduce the combustion reactivity of hydrochars.

### Correlation between combustion reactivity and characteristics of samples

In many studies, comprehensive combustion characteristic index ( $S$ ) was used to indicate reactivity of the samples. The smaller the  $S$  value, the better the reactivity of the sample is reflected. Graphical illustrations of the correlations between chemical structure characteristics and combustion reactivities with the correlation equations are shown in Fig. 7. For all samples,  $I_{D3+D4}/I_G$  showed linear correlations with  $S$ . In addition, with the decrease of  $I_{D3+D4}/I_G$ , the value of  $S$  gradually decreases. In these observations, the degree of order can govern the reactivity of different hydro-char samples. Relatively good fitting results of  $I_{D3+D4}/I_G$  with  $S$  suggest

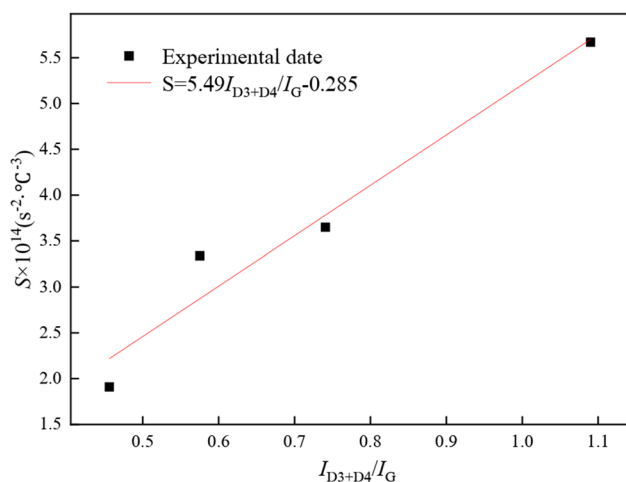


**Fig. 7** The correlation between chemical structure characteristics with combustion reactivities

that carbonaceous structure is the significant factor influencing combustion reactivity of hydro-char. The combustion reactivities of the investigated feedstocks can be predicted from  $I_{D3+D4}/I_G$  in this study. The combustion reactivities of the investigated feedstocks can be predicted from  $I_{D3+D4}/I_G$  in this study.

### Kinetic analysis and estimated activation energy

The weight loss (TG) and rate of weight loss (DTG) curves of the HC hydrochar at the heating rates of 5, 10, and 20 °C/min are shown in Fig. 8.

From the TG and DTG curves, it can be seen that the combustion process of HC and HC hydrochars can be divided into three separate stages: (1) the evaporation stage of water and the low-boiling organic material; (2) the combustion stage of the volatile; and (3) the combustion stage of the fixed carbon (Khan et al. 2009). The results show that the ignition temperature ( $T_i$ ), the peak temperature ( $T_m$ ), and the burnout temperature ( $T_p$ ) tend to be delayed towards high temperature with increasing heating rates due to thermal conductivity. The increasing thermal conductivity leads to an increase in the burning rate (Ma et al. 2017); therefore, the higher temperature difference between the inside and outside of the samples, the decomposition would be faster and the combustion temperature would be higher in the same combustion stage, which is similar to the results of previous studies (Maiti et al. 2007; Zhu et al. 2019). As shown in Table 5, the comprehensive combustion characteristic index  $S$  of the same sample increases with the increase of the heating rate  $\beta$ . The  $S \times 10^{14}$  increased from 0.3430 to 5.6719 ( $s^{-2} \cdot ^\circ C^{-3}$ ) for HC-240 hydrochar particles, while HC-270 hydrochar particles increased from 0.3603 to 3.6474 ( $s^{-2} \cdot ^\circ C^{-3}$ ), and 0.4175 to 3.3381 ( $s^{-2} \cdot ^\circ C^{-3}$ ) of HC-300 hydrochar particles. From the above results, it can be inferred that a high TG heating rate promotes the decomposition and combustion of cellulose, hemicellulose, and lignin in the corncob, thus increasing  $\beta$  can obtain a larger  $S$  value. The combustibility index  $S$  can be used to evaluate fuel combustion characteristic. The

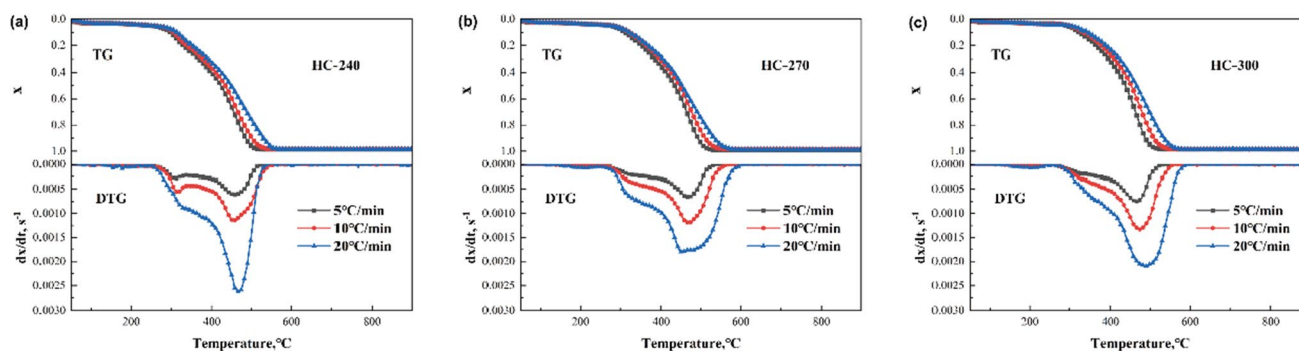


**Fig. 8** TG, DTG curves of (a) HC-240 hydrochar, (b) HC-270 hydrochar, (c) HC-300 hydrochar

combustibility index  $S$  of HC-240 was higher than HC-300, which was associated with the higher volatile matter in raw HC-240, leading to a higher  $DTG_{max}$  of HC-240 than hydrochars. It can be seen from Table 5 that HC-240 has better combustion performance.

A total of 21 conversion rates from 0.01 to 0.99 were selected, 0.1, 0.15, 0.2, 0.25, 0.3, 0.35, 0.4, 0.45, 0.5, 0.55, 0.6, 0.65, 0.7, 0.75, 0.8, 0.85, 0.9. The combustion processes

of the HC hydrochar were analyzed by the KAS and FWO methods. Through the calculation of thermodynamic model, dynamic fitting curve can be concluded (correlation coefficient  $R^2 > 0.9$ ). The linear fitting plots of the two kinetics methods are shown in Figs. 9 and 10, respectively.

Figure 11 shows the relationship between the  $E_\alpha$  and various conversion rates. The  $E_\alpha$  value calculated by KAS is consistent with that calculated by FWO. The  $E_\alpha$  values

**Table 5** The combustion characteristics parameters of HC hydrochars at 5, 10, and 20 °C/min

Sample	$\beta$ (°C/min)	$T_i$ (°C)	$T_m$ (°C)	$T_f$ (°C)	$(dx/dt)_{max}$ (s <sup>-1</sup> )	$(dx/dt)_{max_2}$ (s <sup>-1</sup> )	$(dx/dt)_{mean}$ (s <sup>-1</sup> )	$C \times 10^8$ (s <sup>-1</sup> ·°C <sup>-2</sup> )	$S \times 10^{14}$ (s <sup>-2</sup> ·°C <sup>-3</sup> )
HC-240	5	246.3	422.2	497.1	0.0006	0.0003	1.67E-04	1.0189	0.3430
	10	253.6	434.7	517.3	0.0011	0.0006	3.64E-04	1.7851	2.0503
	20	276.8	434.8	504.6	0.0026	-	8.32E-04	3.4402	5.6719
HC-270	5	267.6	434.2	503.7	0.0007	-	1.95E-04	0.9296	0.3603
	10	278.6	446.9	526.1	0.0012	-	3.79E-04	1.5381	1.1085
	20	281.4	462.6	540.6	1.79E-03	-	8.72E-04	2.2602	3.6474
HC-300	5	293.4	436.9	499.4	7.60E-04	-	2.36E-04	0.8825	0.4175
	10	297.4	452.3	524.4	0.0013	-	3.89E-04	1.5155	1.1243
	20	299.2	464.8	550.4	0.0021	-	7.81E-04	2.3512	3.3381

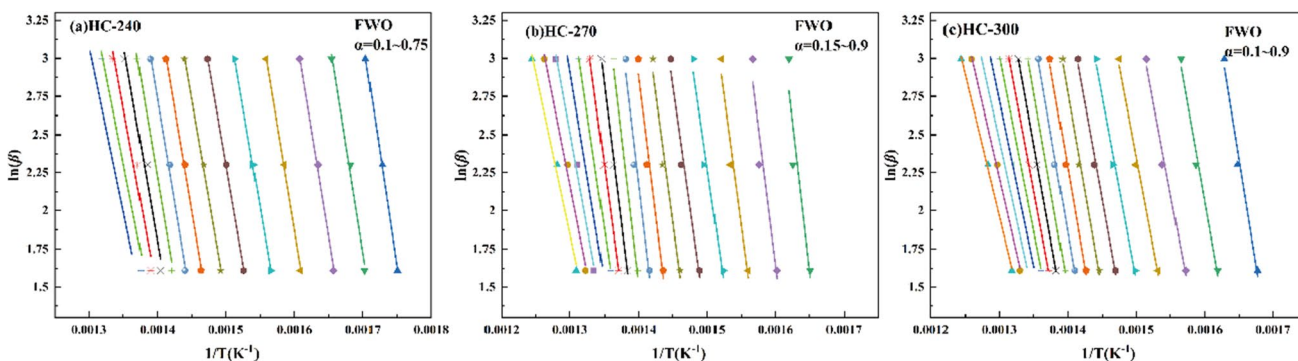


**Fig. 9** Isoconversional plots of (a) HC-240, (b) HC-270, (c) HC-300 combustion at different conversions via the FWO method

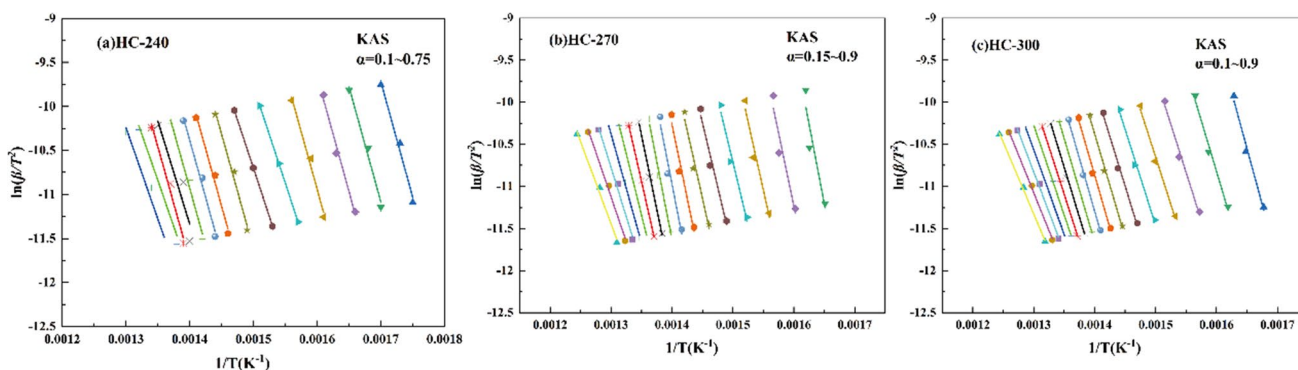


**Fig. 10** Isoconversional plots of (a) HC-240, (b) HC-270, (c) HC-300 combustion at different conversions via the KAS method

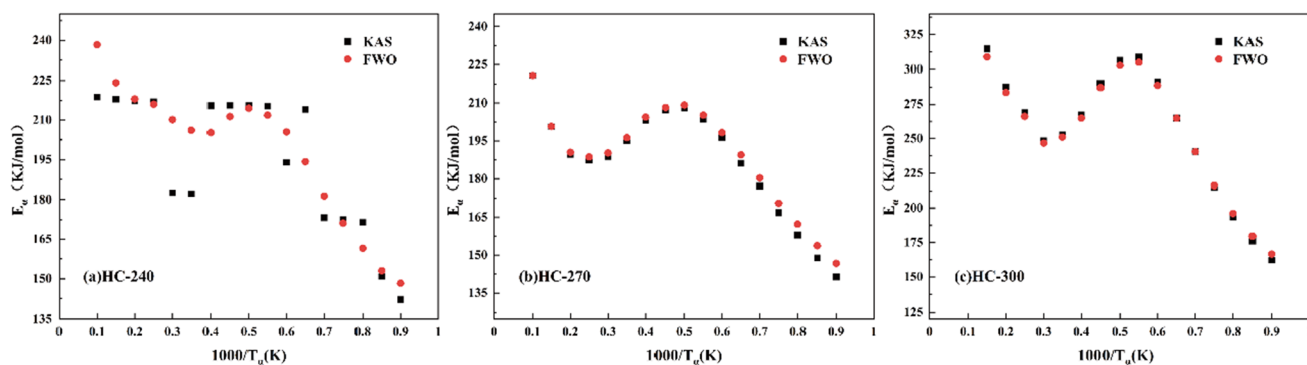


**Fig. 11** The relationship between the  $E_{\alpha}$  and various conversion rates determined via the KAS and FWO methods

**Table 6** Average values of activation energy via KAS and FWO methods

Sample	$E_{\alpha}$ (kJ/mol)	
	KAS	FWO
240	195	198
270	187	189
300	262	262

of the three samples obtained by the two methods are similar, and the  $E_{\alpha}$  values by FWO is slightly larger than that calculated by KAS. As the hydrothermal temperature increases, the difference between the activation energy values obtained by the two calculation methods decreases, indicating that the degree of carbon sorting is also gradually stable and increasing. The changing trend of activation energy is hump-shaped and reaches the maximum value around  $\alpha = 0.1$  and  $\alpha = 0.5$ . When the reaction conversion rate is low in the range of  $\alpha = 0-0.3$ , the activation energy first increases and then decreases with the progress of the reaction. The weak chains on hemicellulose first decompose and break, and then the straight-chain breaks randomly, and  $E$  increases. In the stage of  $\alpha = 0.3-0.99$ , the activation energy increases mainly because lignin begins to decompose. Higher HTC temperature leads to a more complete and deeper hydrothermal reaction.

The  $E_{\alpha}$  of hydrochars are calculated according to Eq. (15) and Eq. (16), and the average value of  $E_{\alpha}$  is calculated. The results are shown in Table 6. It shows that the average correlation coefficient calculated by the FWO method is higher than that calculated by the KAS method, indicating that the FWO method is more suitable for describing the combustion reaction of HC hydrochar particles. Because the average correlation coefficient ( $R^2$ ) is greater than 0.9 in all samples, both the KAS and FWO methods can reliably describe the combustion reaction process (Sait et al. 2012).

## Conclusions

In this study, HTC method was used to produce HC hydrochar as fuel. Proximate analysis, TG/DTG, FTIR and Raman analysis were used. With the increase of HTC temperature and water reused times, the yield of the hydrothermal reaction decreased, the H/C and O/C values decreased, and the HHV increased. The carbon content and HHV of hydrochar reached 67.99–78.51 wt.% and 24.36–27.49 MJ/kg, respectively. HTC treatment can effectively remove alkali metal elements, and the removal efficiency of K reaches 99%. The analysis of physical properties and combustion characteristics showed that the higher the carbon structure order of the hydrothermal carbon, the weaker the combustion reactivity. The combustion of hydrochar will be more stabilized when the HTC temperature increases. Meanwhile, with the increase in hydrothermal temperature and water-reused times, the carbonization ordering degree of HC hydrochar increases. HTC conditions at 300 °C and twice the amount of reused water was found to produce the best biofuels, as well as a higher HHV value than that of bituminous coal.

**Author contribution** All authors contributed to the study's conception and design. Methodology: [Qi An] and [Qi Wang]. Formal analysis and investigation: [Qi An] and [Qi Wang]. Material preparation, data collection and analysis: [Qi An]. Writing—review and editing: [Jinpeng Zhai]. All authors read and approved the final manuscript.

**Data availability** The authors declare that the data supporting the findings of this study are available within this article.

## Declarations

**Competing interests** The authors have no relevant financial or non-financial interests to disclose.



## References

- Abdul Quader M, Ahmed S, Dawal SZ, Nukman Y (2016) Present needs, recent progress and future trends of energy-efficient Ultra-Low Carbon Dioxide (CO<sub>2</sub>) Steelmaking (ULCOS) program. *Renew Sustain Energy Rev* 55:537–549. <https://doi.org/10.1016/J.RSER.2015.10.101>
- Channiwalla SA, Parikh PP (2002) A unified correlation for estimating HHV of solid, liquid and gaseous fuels. *Fuel* 81:1051–1063. [https://doi.org/10.1016/S0016-2361\(01\)00131-4](https://doi.org/10.1016/S0016-2361(01)00131-4)
- Chen WH, Cheng WY, Lu KM, Huang YP (2011) An evaluation on improvement of pulverized biomass property for solid fuel through torrefaction. *Appl Energy* 88:3636–3644. <https://doi.org/10.1016/J.APENERGY.2011.03.040>
- Chen WH, Lin BJ, Huang MY, Chang JS (2015) Thermochemical conversion of microalgal biomass into biofuels: a review. *Bioresour Technol* 184:314–327. <https://doi.org/10.1016/J.BIORTECH.2014.11.050>
- Crutzen PJ, Mosier AR, Smith KA, Winiwarter W (2008) N<sub>2</sub>O release from agro-biofuel production negates global warming reduction by replacing fossil fuels. *Atmos Chem Phys* 8:389–395. <https://doi.org/10.5194/ACP-8-389-2008>
- da Silva Machado JGM, Osório E, Faria Vilela AC (2010) Reactivity of Brazilian coal, charcoal, imported coal and blends aiming to their injection into blast furnaces. *Mater Res* 13:287–292. <https://doi.org/10.1590/S1516-14392010000300003>
- Ding L, Zou B, Liu H et al (2013) A new route for conversion of corncob to porous carbon by hydrolysis and activation. *Chem Eng J* 225:300–305. <https://doi.org/10.1016/J.CEJ.2013.03.090>
- Falco C, Sieben JM, Brun N et al (2013) Hydrothermal carbons from hemicellulose-derived aqueous hydrolysis products as electrode materials for supercapacitors. *Chemosuschem* 6:374–382. <https://doi.org/10.1002/CSSC.201200817>
- Fong MJB, Loy ACM, Chin BLF et al (2019) Catalytic pyrolysis of *Chlorella vulgaris*: kinetic and thermodynamic analysis. *Bioresour Technol* 289:121689. <https://doi.org/10.1016/J.BIORTECH.2019.121689>
- Funke A, Reeb F, Kruse A (2013) Experimental comparison of hydrothermal and vapothermal carbonization. *Fuel Process Technol* 115:261–269. <https://doi.org/10.1016/J.FUPROC.2013.04.020>
- Gao Y, Wang X, Wang J et al (2013) Effect of residence time on chemical and structural properties of hydrochar obtained by hydrothermal carbonization of water hyacinth. *Energy* 58:376–383. <https://doi.org/10.1016/J.ENERGY.2013.06.023>
- Gao Y, Yu B, Wang X et al (2015) Orthogonal test design to optimize products and to characterize heavy oil via biomass hydrothermal treatment. *Energy* 88:139–148. <https://doi.org/10.1016/J.ENERGY.2015.04.014>
- Gao P, Zhou Y, Meng F et al (2016) Preparation and characterization of hydrochar from waste eucalyptus bark by hydrothermal carbonization. *Energy* 97:238–245. <https://doi.org/10.1016/J.ENERGY.2015.12.123>
- Khan AA, de Jong W, Jansens PJ, Spliethoff H (2009) Biomass combustion in fluidized bed boilers: potential problems and remedies. *Fuel Process Technol* 90:21–50. <https://doi.org/10.1016/J.FUPROC.2008.07.012>
- Kizgut S, Yilmaz S (2004) Characterization and non-isothermal decomposition kinetics of some Turkish bituminous coals by thermal analysis. *Fuel Process Technol* 85:103–111. [https://doi.org/10.1016/S0378-3820\(03\)00111-5](https://doi.org/10.1016/S0378-3820(03)00111-5)
- Lee J, Lee K, Sohn D et al (2018) Hydrothermal carbonization of lipid extracted algae for hydrochar production and feasibility of using hydrochar as a solid fuel. *Energy* 153:913–920. <https://doi.org/10.1016/J.ENERGY.2018.04.112>
- Li XG, Lv Y, Ma BG et al (2011) Thermogravimetric investigation on co-combustion characteristics of tobacco residue and high-ash anthracite coal. *Bioresour Technol* 102:9783–9787. <https://doi.org/10.1016/J.BIORTECH.2011.07.117>
- Li J, Pan L, Suvarna M, et al (2020) Fuel properties of hydrochar and pyrochar: prediction and exploration with machine learning. *Appl Energy* 269. <https://doi.org/10.1016/j.apenergy.2020.115166>
- Lin Y, Ma X, Peng X et al (2015) Effect of hydrothermal carbonization temperature on combustion behavior of hydrochar fuel from paper sludge. *Appl Therm Eng* 91:574–582. <https://doi.org/10.1016/J.APPLTHERMALENG.2015.08.064>
- Lin Y, Xu H, Gao Y, Zhang X (2021) Preparation and characterization of hydrochar-derived activated carbon from glucose by hydrothermal carbonization. *Biomass Convers Biorefin* 1–12. <https://doi.org/10.1007/S13399-021-01407-Y/FIGURES/10>
- Liu Z, Quek A, Kent Hoekman S et al (2012) Thermogravimetric investigation of hydrochar-lignite co-combustion. *Bioresour Technol* 123:646–652. <https://doi.org/10.1016/J.BIORTECH.2012.06.063>
- Liu Y, Li W, Chen Y (2022) Synthesis of MOF derivatives@3D graphene hybrid materials towards high-performance electrode material for supercapacitors. *J Mater Sci: Mater Electron* 33:6514–6523. <https://doi.org/10.1007/S10854-022-07826-5/FIGURES/7>
- Lokahita B, Aziz M, Yoshikawa K, Takahashi F (2017) Energy and resource recovery from Tetra Pak waste using hydrothermal treatment. *Appl Energy* 207:107–113. <https://doi.org/10.1016/J.APENERGY.2017.05.141>
- Ma P, Yang J, Xing X et al (2017) Isoconversional kinetics and characteristics of combustion on hydrothermally treated biomass. *Renew Energy* 114:1069–1076. <https://doi.org/10.1016/J.RENENE.2017.07.115>
- Maiti S, Purakayastha S, Ghosh B (2007) Thermal characterization of mustard straw and stalk in nitrogen at different heating rates. *Fuel* 86:1513–1518. <https://doi.org/10.1016/J.FUEL.2006.11.016>
- Mäkelä M, Volpe M, Volpe R et al (2018) Spatially resolved spectral determination of polysaccharides in hydrothermally carbonized biomass. *Green Chem* 20:1114–1120. <https://doi.org/10.1039/C7GC03676K>
- Mau V, Neumann J, Wehrli B, Gross A (2019) Nutrient behavior in hydrothermal carbonization aqueous phase following recirculation and reuse. *Environ Sci Technol* 53:10426–10434. <https://doi.org/10.1021/acs.est.9b03080>
- McGlade C, Ekins P (2015) The geographical distribution of fossil fuels unused when limiting global warming to 2 °C. *Nature* 517:187–190. <https://doi.org/10.1038/NATURE14016>
- Mosqueda A, Wei J, Medrano K et al (2019) Co-gasification reactivity and synergy of banana residue hydrochar and anthracite coal blends. *Appl Energy* 250:92–97. <https://doi.org/10.1016/J.APENERGY.2019.05.008>
- Mumme J, Eckervogt L, Pielert J et al (2011) Hydrothermal carbonization of anaerobically digested maize silage. *Bioresour Technol* 102:9255–9260. <https://doi.org/10.1016/J.BIORTECH.2011.06.099>
- Nzediegwu C, Naeth MA, Chang SX (2021) Carbonization temperature and feedstock type interactively affect chemical, fuel, and surface properties of hydrochars. *Bioresour Technol* 330:124976. <https://doi.org/10.1016/J.BIORTECH.2021.124976>
- Park SW, Jang CH (2011) Characteristics of carbonized sludge for co-combustion in pulverized coal power plants. *Waste Manage* 31:523–529. <https://doi.org/10.1016/J.WASMAN.2010.10.009>
- Patrinoiu G, Calderon-Moreno JM, Birjega R, Carp O (2015) Solid vs. hollow oxide spheres obtained by hydrothermal carbonization of various types of carbohydrates. *RSC Adv* 5:31768–31771. <https://doi.org/10.1039/C5RA03447G>
- Peng C, Zhai Y, Zhu Y et al (2016) Production of char from sewage sludge employing hydrothermal carbonization: char properties, combustion behavior and thermal characteristics. *Fuel* 176:110–118. <https://doi.org/10.1016/J.FUEL.2016.02.068>

- Prawisudha P, Namioka T, Yoshikawa K (2012) Coal alternative fuel production from municipal solid wastes employing hydrothermal treatment. *Appl Energy* 90:298–304. <https://doi.org/10.1016/J.APENERGY.2011.03.021>
- Rajarao R, Mansuri I, Dhunna R et al (2014) Characterisation of gas evolution and char structural change during pyrolysis of waste CDs. *J Anal Appl Pyrolysis* 105:14–22. <https://doi.org/10.1016/J.JAAP.2013.09.014>
- Reza MT, Mumme J, Ebert A (2015a) Characterization of hydrochar obtained from hydrothermal carbonization of wheat straw digestate. *Biomass Convers Biorefin* 5:425–435. <https://doi.org/10.1007/S13399-015-0163-9/FIGURES/4>
- Reza MT, Rottler E, Herklotz L, Wirth B (2015b) Hydrothermal carbonization (HTC) of wheat straw: influence of feedwater pH prepared by acetic acid and potassium hydroxide. *Bioresour Technol* 182:336–344. <https://doi.org/10.1016/J.BIORTECH.2015.02.024>
- Sait HH, Hussain A, Salema AA, Ani FN (2012) Pyrolysis and combustion kinetics of date palm biomass using thermogravimetric analysis. *Bioresour Technol* 118:382–389. <https://doi.org/10.1016/J.BIORTECH.2012.04.081>
- Seredych M, Hulicova-Jurcakova D, Lu GQ, Bandosz TJ (2008) Surface functional groups of carbons and the effects of their chemical character, density and accessibility to ions on electrochemical performance. *Carbon N Y* 46:1475–1488. <https://doi.org/10.1016/J.CARBON.2008.06.027>
- Tekin K, Karagöz S, Bektaş S (2014) A review of hydrothermal biomass processing. *Renew Sustain Energy Rev* 40:673–687. <https://doi.org/10.1016/J.RSER.2014.07.216>
- Titirici MM, Antonietti M (2009) Chemistry and materials options of sustainable carbon materials made by hydrothermal carbonization. *Chem Soc Rev* 39:103–116. <https://doi.org/10.1039/B819318P>
- Trninic M, Jovic A, Stojiljkovic D (2016) A steady state model of agricultural waste pyrolysis: a mini review. *Waste Manage Res* 34:851–865. <https://doi.org/10.1177/0734242X16649685>
- Uddin MH, Reza MT, Lynam JG, Coronella CJ (2014) Effects of water recycling in hydrothermal carbonization of loblolly pine. *Environ Prog Sustain Energy* 33:1309–1315. <https://doi.org/10.1002/EP.11899>
- Várhegyi G (2007) Aims and methods in non-isothermal reaction kinetics. *J Anal Appl Pyrolysis* 79:278–288. <https://doi.org/10.1016/J.JAAP.2007.01.007>
- Wagner A, Kaupenjohann M (2014) Suitability of biochars (pyro- and hydrochars) for metal immobilization on former sewage-field soils. *Eur J Soil Sci* 65:139–148. <https://doi.org/10.1111/EJSS.12090>
- Wang T, Zhai Y, Zhu Y et al (2018) Evaluation of the clean characteristics and combustion behavior of hydrochar derived from food waste towards solid biofuel production. *Bioresour Technol* 266:275–283. <https://doi.org/10.1016/J.BIORTECH.2018.06.093>
- Wang G, Ren S, Zhang J et al (2020a) Influence mechanism of alkali metals on CO<sub>2</sub> gasification properties of metallurgical coke. *Chem Eng J* 387:124093. <https://doi.org/10.1016/J.CEJ.2020.124093>
- Wang G, Zhang J, Lee JY et al (2020b) Hydrothermal carbonization of maize straw for hydrochar production and its injection for blast furnace. *Appl Energy* 266:114818. <https://doi.org/10.1016/J.APENERGY.2020.114818>
- Wang G, Li D, Xiong L, et al (2023) Application of catalysts in biomass hydrothermal carbonization for the preparation of high-quality blast furnace injection fuel. *Energy* 283. <https://doi.org/10.1016/j.energy.2023.129147>
- Wu S, Wang Q, Cui D et al (2023) Analysis of fuel properties of hydrochar derived from food waste and biomass: evaluating varied mixing techniques pre/post-hydrothermal carbonization. *J Clean Prod* 430:139660. <https://doi.org/10.1016/j.jclepro.2023.139660>
- Xu Y, Zhang C, Xia J et al (2010) Experimental study on the comprehensive behavior of combustion for blended coals. *Asia-Pac J Chem Eng* 5:435–440. <https://doi.org/10.1002/APJ.264>
- Yong LF, Hui SJ, Gang ZZ (2012) Effect of the alkali metals' existing form on its emission characteristics during biomass combustion process. *Adv Mat Res* 550–553:544–549. <https://doi.org/10.4028/WWW.SCIENTIFIC.NET/AMR.550-553.544>
- Zhang L, Wang Q, Wang B et al (2015) Hydrothermal carbonization of corn cob residues for hydrochar production. *Energy Fuels* 29:872–876. <https://doi.org/10.1021/EF502462P>
- Zhao P, Ge S, Yoshikawa K (2013) An orthogonal experimental study on solid fuel production from sewage sludge by employing steam explosion. *Appl Energy* 112:1213–1221. <https://doi.org/10.1016/J.APENERGY.2013.02.026>
- Zhou Y, Shi W, Engler N, Nelles M (2021) High-value utilization of kitchen waste derived hydrochar in energy storage regulated by circulating process water. *Energy Convers Manag* 229:113737. <https://doi.org/10.1016/J.ENCONMAN.2020.113737>
- Zhu X, Li X, Xiao L et al (2016) Novel carbon-rich additives preparation by degradative solvent extraction of biomass wastes for coke-making. *Bioresour Technol* 207:85–91. <https://doi.org/10.1016/J.BIORTECH.2016.01.105>
- Zhu G, Yang L, Gao Y et al (2019) Characterization and pelletization of cotton stalk hydrochar from HTC and combustion kinetics of hydrochar pellets by TGA. *Fuel* 244:479–491. <https://doi.org/10.1016/J.FUEL.2019.02.039>

**Publisher's Note** Springer Nature remains neutral with regard to jurisdictional claims in published maps and institutional affiliations.

Springer Nature or its licensor (e.g. a society or other partner) holds exclusive rights to this article under a publishing agreement with the author(s) or other rightsholder(s); author self-archiving of the accepted manuscript version of this article is solely governed by the terms of such publishing agreement and applicable law.